Anal. Chem. **2006,** *78,* 8347−8353

Surface and Depth Profiling Investigation of a Drug-Loaded Copolymer Utilized To Coat Taxus Express^2 Stents

Robert M. Braun,*,† Juan Cheng,‡ Edward E. Parsonage,§ Jeff Moeller,§ and Nicholas Winograd‡

Polymer and Surface Science Group, Bausch & Lomb Inc., 1400 North Goodman Street, Rochester, New York 14609, Chemistry Department, Pennsylvania State University, 104 Chemistry Building, University Park, Pennsylvania 16802, and Boston Scientific Inc., One SciMed Place, Maple Grove, Minnesota 55311-1566

The surface of a styrene-*b*-isobutylene-*b*-styrene triblock copolymer, containing a solid-phase drug, was studied by time-of-flight secondary ion mass spectrometry employing 15-keV Ga^+ and 20-keV C_{60}^+ ion sources. This polymer/drug system has direct application in the cardiac stent arena, where it has been used to treat restenosis or renarrowing of arterial walls after stent or angioplasty procedures. Overall, the results illustrate the successful use of a cluster ion beam for greatly enhancing the high-mass fragment ion and molecular ion intensities from the surface and bulk of the polymer system. The use of C_{60}^+ also established the ability to remove common overlayers like poly(dimethylsiloxane), which was not possible using a Ga^+ ion source. Furthermore, the use of C_{60}^+ allowed depth profiles to be obtained using primary ion dose densities in excess of 6×10^{14} C_{60}^+/cm^2. Resultant sputter craters reached depths of ~ 2 μm and possessed relatively flat bottoms without the need for sample rotation. AFM and profilometry studies support the relatively gentile removal of surface species via phase contrast and topographic imaging. In addition, the findings suggest that relatively high ion doses do not significantly alter the phase distribution or surface topography of the polymer surface; however, a slight increase in surface roughness was detected.

Recently, the general use and understanding of polymeric biomaterials utilized within in vivo applications has dramatically increased. The use of degradable and nondegradable materials has led to the incorporation of hydrogels[1] and derivatives of poly(lactic acid)[2], poly(glycolic acid),[3] and poly(ethylene glycol)[4] into a variety of drug delivery applications.[5−8] Furthermore, the use of polymeric systems as grafting agents and passivation layers has extended the overall applicability of current materials.[9−11] While the applications of polymer coatings and materials are immense, the work in this study will focus on the characterization of a nondegradable polymer coating associated with implantable stent technology.

Stents themselves are precisely engineered, tubular supports that are commonly used within fluid transport vessels like arteries and veins to open restrictions caused by the growth of tissue or accumulation of deposits found within bodily fluids.[12] For instance, the accumulation of material within a coronary artery is shown schematically in Figure 1a.[13] In this case, plaque buildup within the artery has caused a restriction that could ultimately reduce blood flow to dangerously low levels. The need for a reasonably strong support system to reopen the restriction has required the use of stents made from metals such as NiTi (nitinol) and stainless steel alloys that are flexible, strong, and offer an innate level of biocompatibility, eliminating the need for protective coatings. Because of their ability to be expanded and retain their shape, stents have recently become ideal mechanical remedies for a variety of complex chemical problems within the body.[14] Prior to delivery within the body, stents are collapsed around the end of a long, balloon-tipped catheter. Once the catheter is positioned within a given vessel, the balloon is expanded, which simultaneously expands the stent diameter. Deflating the balloon and subsequently withdrawing the catheter leaves the stent behind to support the surrounding tissue and increase fluid transport (Figure 1b).[15] However, it has been found that, upon stent implantation, the body's natural defense mechanisms respond by encapsulating the metallic lattice via enhanced tissue growth in

* To whom correspondence should be addressed. E-mail: rbraun@bausch.com.
† Bausch & Lomb Inc.
‡ Pennsylvania State University.
§ Boston Scientific Inc.

(1) Bae, Y. H.; Huh, K. M.; Kim, Y.; Park, K. H. *J. Controlled Release* **2000**, *64*, 3−13.
(2) Mathiowitz, E. *The Encyclopedia of Controlled Drug Delivery*; Wiley: New York, 1999.
(3) Park, H.; Park, K. In *Polymers of Biological and Biomedical Significance*; Shalaby, S. W., Ed.; ACS Symposium Series 540; American Chemical Society: Washington, DC, 1994; pp 1−15.
(4) Shard, A. G.; Clarke, S.; Davies, M. C. *Surf. Int. Anal.* **2002**, *33*, 528−532.
(5) Dechy-Cabaret, O.; Martin-Vaca, B.; Bourissou, D. *Chem. Rev.* **2004**, *104*, 6147−6176.
(6) Huh, K. M.; Cho, Y. W.; Park, K. *Drug Delivery Technol.* **2003**, *3*, 42−49.
(7) Yasukawa, T.; Ogura, Y.; Tabata, Y.; Kimura, H.; Wiedemann, P.; Honda, Y. *Prog. Retinal Eye Res.* **2004**, *23*, 253−281.
(8) Malmsten, M. *Surfactants and Polymers in Drug Delivery*; Drugs and the Pharmaceutical Sciences Vol. 122, Marcel Dekker: Inc.: New York, 2002.
(9) Khan, F. *Biomacromoles* **2004**, *5* (3), 1078−1088.
(10) Hu, S.; Ren, X.; Bachman, M.; Sims, C. E.; Li, G. P.; Allbritton, N. *Anal. Chem.* **2002**, *74* (16), 4117−4123.
(11) Meier, M. A. R.; Schubert, U. S. *J. Comb. Chem.* **2005**, *7* (3), 356−359.
(12) Al Suwaidi, J.; Berger, P. B.; Holmes, D. R. *J. Am. Med. Assoc.* **2000**, *284*, 1828−1836.
(13) Adapted from Hartford Health Services, http://www.harthosp.org.
(14) Serruys, P. W.; de Jaegere, P.; Kiemeneij, F.; Macaya, C.; Rutsch, W.; Heyndrickx, G.; Emanuelsson, H.; Marco, J.; Legrand, V.; Materne, P. *N. Engl. J. Med.* **1994**, *331*, 489−495.
(15) Adapted from Fairview Health Services, http://www.fairview.org.

10.1021/ac0615089 CCC: $33.50
Published on Web 11/10/2006

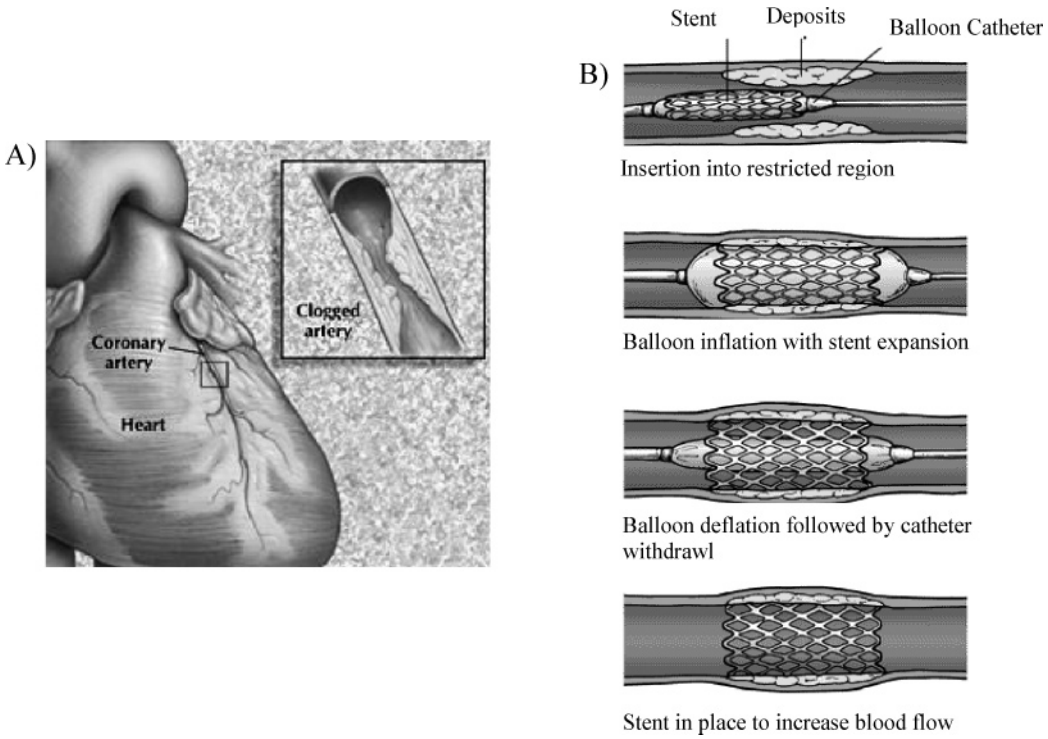

Figure 1. Schematic depiction of narrowing in coronary artery (A) and method of stent delivery and placement within restriction (B).

and around the device. Unfortunately, this often leads to a renarrowing of the passage, which is referred to as neointimal hyperplasia and classified as restenosis.[16] Complications associated with restenosis may occur within months of device implantation and can limit the useful lifetime of the device. Consequently, the routine use of uncoated stents has proven to be short-lived within the biomedical industry and has led to the development of more advanced systems.[17]

Although it is possible to abate the buildup of red/white blood cells as well as plaque within arteries using pharmaceutical products, slowing tissue growth in and around implanted devices presents a much greater challenge. The use of oral and intravenous drugs to control tissue growth associated with such small contact areas would require sustained doses that may have deleterious effects on other systems within the body. Interestingly, these challenges have recently been overcome by introducing a drug within a biocompatible polymer matrix that is coated onto the exposed surfaces of a given stent. Localized coatings of this nature allow for the sustained release of drugs that delay or eliminate the onset of tissue growth resulting in a reduction or elimination of restenotic pathways.[18]

It is possible to interrogate the surfaces of these complex biomaterials using time-of-flight secondary ion mass spectrometry (TOF-SIMS).[19,20] However, the use of monatomic sources (i.e., Ga^+) to probe the surface and bulk structures of these materials has been limited. Low primary ion doses often lead to low secondary ion detection sensitivities while higher ion doses transfer large amounts of energy to the solid resulting in damage accumulation and loss of secondary ion signals.[21−23] In comparison, recent advances in the development of cluster ion sources have significantly enhanced detection sensitivities and minimized beam-induced damage in organic and polymeric matrixes. The multiatom structure of these cluster ions (e.g., SF_5^+ and C_{60}^+) allows impact energies to be partitioned among the atoms, resulting in more efficient energy transfer to the topmost layers of the solid.[24] As a result, sputter yields have increased dramatically, resulting in greater detection sensitivities of high-mass species and less damage accumulation during the ion bombardment process.[25−27] These exciting discoveries allow the three-dimensional structure of most organic and polymer samples to be investigated with enhanced depth resolution and without the degree of damage associated with monatomic ion sources.[28−30] Recent developments have also lead this field into the characterization of drug-containing polymers, including coated stents.[31,32]

In this study, we examine the distribution of chemical species present on the surface and as a function of depth on the Taxus

(16) Costa, M. A.; Foley, D. P.; Serruys, P. W. In *Practical interventional cardiology*, 2nd ed.; Gretch, E. D., Ramsdale, D. R., Eds.; Martin Dunitz: London, 2002; pp 279−294.
(17) Patel, S. J.; Perera, D.; Redwood, S. R. *J. Renovasc. Dis.* **2003**, *2*, 17−33.
(18) Richards, R. E.; Ranade, S. V.; Schwarz, M. C.; Barry, J. J.; Kamath, K.; Miller, K. *Proceedings of Surfaces in Biomaterials Foundation Symposium*, 2004; p 58.
(19) Benninghoven, A. In *TOF-SIMS: Surface Analysis by Mass Spectrometry*; Vickerman, J. C., Briggs, D., Eds.; IM Publications: London, England, 2001; pp 41−74.
(20) Benninghoven, A.; Hagenhoff, B.; Niehuis, E. *Anal. Chem.* **1993**, *65*, 630A−640A.
(21) Briggs, D; Hearn, M. J.; Ratner, B. D. *Surf. Interface Anal.* **1984**, *6*, 184−192.
(22) Leggett, G. J.; Vickerman, J. C. *Appl. Surf. Sci.* **1992**, *55*, 105−115.
(23) Gilmore, I. S.; Seah, M. P. *Surf. Interface Anal.* **1996**, *24*, 746−762.
(24) Appelhans, A. D.; Delmore, J. E. *Anal. Chem.* **1989**, *61*, 1087−1093.
(25) Gillen, G.; Roberson, S. *Rapid Commun. Mass Spectrom.* **1998**, *12*, 1303−1312.
(26) Fuoco, E. R.; Gillen, G.; Wijesundara, M. B. J.; Wallace, W. E.; Hanley, L. *J. Phys. Chem. B* **2001**, *105* (18), 3950−3956.
(27) Weibel, D.; Wong, S.; Lockyer, N.; Blenkinsopp, P.; Hill, R.; Vickerman, J. C. *Anal. Chem.* **2003**, *75*, 1754−1764.
(28) Wagner, M. S. *Anal. Chem.* **2005**, *77*, 911−922.
(29) Sanada, N.; Yamamota, A.; Oiwa, R.; Ohashi, Y. *Surf. Interface Anal.* **2004**, *36*, 280−282.
(30) Mahoney, C. M.; Yu, J.; Gardella, J. A. *Anal. Chem.* **2005**, *77*, 3570−3578.

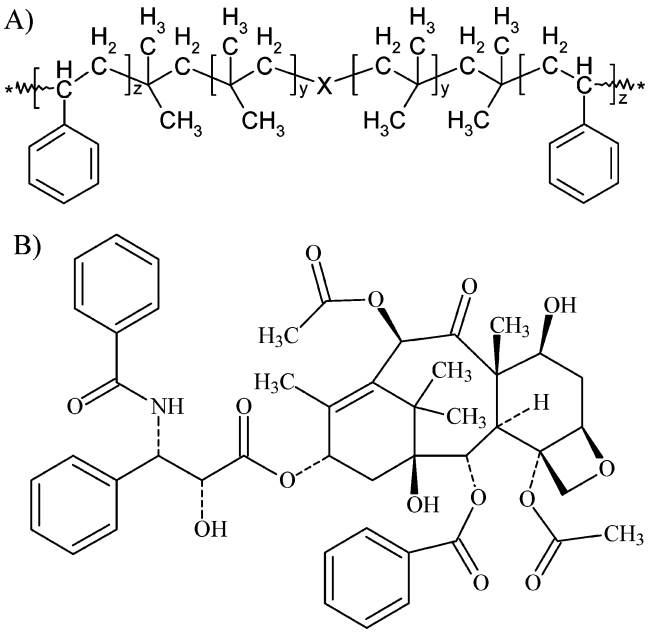

Figure 2. (A) Chemical structure of poly(styrene-*b*-isobutylene-*b*-styrene) (SIBS). Ratios used in this study: 16 mol % PS; 84 mol % PIB. (B) Structure of paclitaxel used in study, MW 854, incorporated at 8 wt %.

Express[2] Paclitaxel-eluting Coronary Stent using SIMS utilizing a C_{60}^+ primary projectile. The results show that surface and bulk distributions of these materials may be examined in detail, minimizing artifacts at higher primary ion doses that are commonly associated with the use of monatomic primary ions like Ga^+. Moreover, surface films, such as poly(dimethylsiloxane), may be removed by cluster bombardment without insulting the underlying chemistry. Changes in the physical nature of the material during and after cluster bombardment are monitored by AFM and profilometry to ensure artifacts such as formation of topographical features and ion beam mixing do not distort the analysis. Discoveries related to the distribution of species within these drug matrixes will lead to a better understanding of existing devices and may help future development efforts that will allow biomaterials to be tailored to specific patient needs.

EXPERIMENTAL SECTION

Sample Preparation and Materials. The generic structure of the proprietary, triblock copolymer system (i.e., Translute polymer) used to coat the Express[2] stents is shown in Figure 2a.[33] Coating formulations characterized in this study contained paclitaxel levels of 0.0 and 8.8% by weight. Crystalline cGMP paclitaxel was obtained from Hauser Inc. (Denver, CO) and used without purification or modification (Figure 2b).

Our initial quality assurance and quality control investigations involved characterizing individual struts on medical grade stents using Ga^+ ion beams. However, the sample handling, alignment, and mounting procedures required to process the samples proved to be possible but a bit cumbersome for expedient development work. Consequently, paclitaxel/SIBS formulations were evaluated using knife cast films. These films helped refine the ion beam characterization process because of the limited sampling areas available on individual stent struts as well as the limited number of accessible struts after the stents were mounted and placed within the SIMS instrument. Film use also reduced the possibility of nonuniform sputtering due to stent/strut tilt angles since it was not always possible to perfectly align the samples orthogonal to the secondary ion flight path. The SIBS films were cast ~500 μm thick from a 75:25 toluene/THF solution onto clean poly(ethylene terephthalate) sheets and have been previously characterized using transmission electron microscopy, scanning electron microscopy, differential scanning calorimetry, X-ray diffraction, and nuclear magnetic resonance spectroscopy and deemed the same as coatings placed on Taxus Express[2] stents.[34]

Secondary Ion Mass Spectrometry. The use and performance of a TRIFT III (Physical Electronics, Chanhassen, MN) TOF-SIMS spectrometer has been described in detail elsewhere and is briefly discussed below.[35] The instrument is equipped with a liquid metal ion source (Ga^+) that was operated at 15 keV using a bunched ion beam. The dc beam current for this source was 2nA. Using pulse widths ranging from 18 to 21 ns, a repetition rate of 10 kHz, and analysis areas of ~125 μm × 125 μm yielded primary ion doses of ~5×10^{12} ions/cm^2 for each of the samples.

Data were also obtained on a BioToF TOF-SIMS instrument that has been described in detail elsewhere and is briefly discussed below.[36] The instrument incorporates a C_{60}^+ primary ion source from Ionoptika Ltd. (Southampton, UK), which is directed at a 40° angle relative to the surface normal. The source is operated at an anode voltage of 20 keV with a 2.0-A electron beam filament current and a 40-V grid voltage. Resulting dc beam currents are 1 nA of pure C_{60}^+ using a 1000-μm beam-defining aperture. During depth profiling, the C_{60}^+ ion beam was operated in dc mode using a range of 300 μm × 300 μm−600 μm × 600 μm areas followed by the acquisition of TOF mass spectra after each sputter cycle using C_{60}^+ at an ion fluence of 10^{10} cm^{-2}. Spectral acquisitions were obtained from regions within the respective sputter craters using raster-field widths approximately one-fourth the width of the crater to avoid potential edge effects. The mass spectrometer was operated in a delayed extraction mode where a delay time of 100 ns was set between the primary ion pulse (duration 50 ns) and the secondary ion extraction pulse. Charge compensation was found to be unnecessary for the positive ion SIMS mode. The value of the signal intensity is calculated from the integrated peak area at the corresponding mass value. It was not possible to effectively utilize negative ion data within this polymer/drug system because of isobaric interferences between the respective components.

AFM Data. A Multimode AFM (Digital Instruments/Veeco Metrology) driven by Nanoscope IIIA and Nanoscope Extender electronics was used to investigate each of the sputtered and control samples associated with the paclitaxel/Translute polymer system. The instrument cantilever was a Tap300 Metrology Probe (Nanodevices, Santa Barbara, CA) that possessed the following features: single-arm silicon; length, 120 μm, spring constant, 40 N/m; resonant frequency, 300 kHz; AFM probe tip, ~10-nm radius

(31) Mahoney, C. M.; Roberson, S. V.; Gillen, G. *Anal. Chem.* **2004**, *76*, 3199−3207.
(32) Mahoney, C. M.; Patwardhan, D. V.; McDermott, M. K. *Appl. Surf. Sci.* **2006**, *252* (19), 6554−6557.
(33) Stone, G. W.; Ellis, S. G.; Cox, D. A.; Hermiller, J.; O'Shaughnessy, C. O.; Mann, J. T.; Turco, M.; Caputo, R.; Bergin, P.; Greenburg, J.; Popma, J.; Russell, M. E. *N. Engl. J. Med.* **2004**, *350*, 221−231.
(34) Ranade, S. V.; Miller, K. M.; Richard, R. E.; Chan, A. K.; Allen, M. J.; Helmus, M. N. *J. Biomed. Mater. Res. A.* **2004**, *71*, 625−634.
(35) Schueler, B. *Microsc. Microanal. Microstruct.* **1992**, *3*, 119−124.
(36) Braun, R. M.; Blenkinsopp, Mullock, S. J.; Corlett, C.; Willey, K. F.; Vickerman, J. C.; Winograd, N. *Rapid Commun. Mass Spectrom.* **1998**, *12*, 1246−1252.

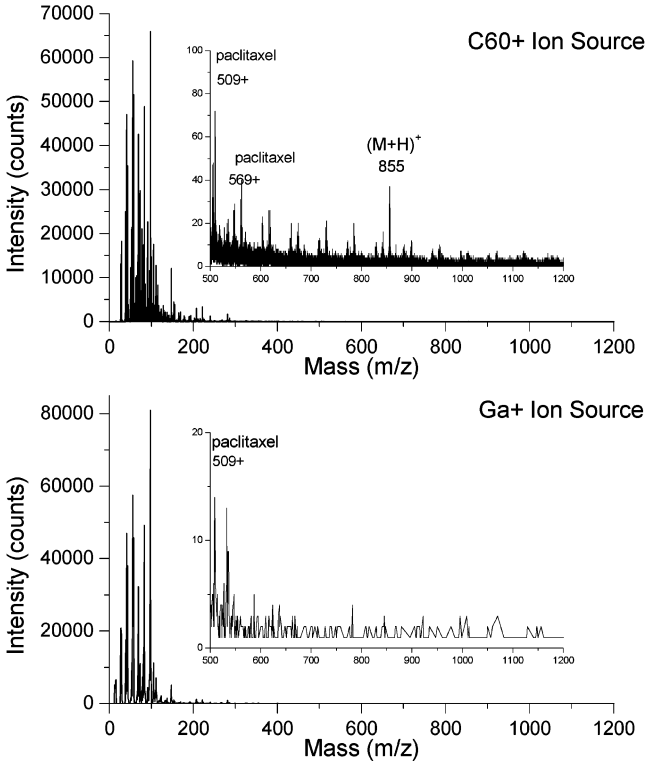

Figure 3. Secondary ion mass spectra of a paclitaxel-loaded SIBS copolymer. The data were generated utilizing Ga^+ ions (lower spectrum) and C_{60}^+ ions (upper spectrum) with primary ion doses $\leq 1 \times 10^{12}$ ions/cm^2. The spectra clearly show detection of higher mass species using C_{60}^+ primary ions.

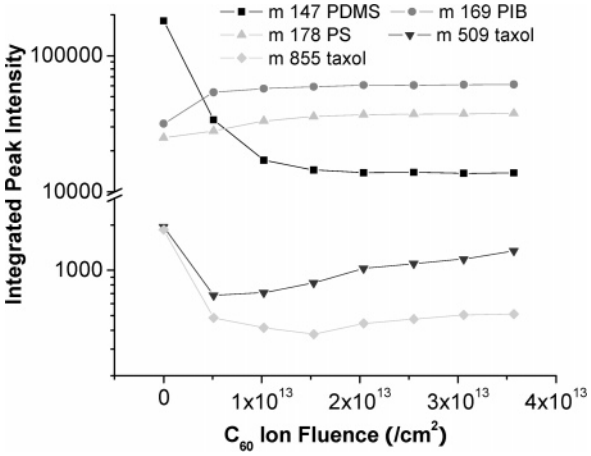

Figure 4. Depth profile of SIBS polymer containing paclitaxel (i.e., Taxol). Secondary ion intensities for select species plotted as a function of C_{60}^+ions/cm^2.

of curvature. Tapping mode measurements were performed by setting the piezodrive amplitude to produce a 4-V near-surface, noncontact cantilever oscillation signal with the contact attenuation set point fixed at 3 V.

AFP Results. Crater analyses, which included depths, edge profiles, and calculated sputter rates were accomplished using a Nanopics2100 atomic force profilometer from KLA-Tencor (San Jose, CA). The metrology tool uses three linear voice coil motors to drive along the *X*, *Y*, and *Z* axes, thus providing large scan fields (up to 800 μm $\times$ 800 μm). Resolution along the *Z* axis and *X*/*Y* ranges are about 0.3 and 2 nm, respectively. Tips used during the reported experiments have the following characteristics: single arm silicon; spring constant, 4 N/m; radius, 20 nm; conical shape with 20° initial angle and 60° at the flare point. The force exerted by the tip on the samples in contact mode is 1150 nN.

RESULTS AND DISCUSSION

Initial investigations involving a paclitaxel-loaded SIBS polymer utilized a Ga^+ ion source to generate secondary ions. As shown in Figure 3 (bottom), it is not possible to obtain a molecular ion (M + H) peak associated with paclitaxel (*m*/*z* 855). The presence of poly(dimethylsiloxane) (PDMS), which is innate to the polymer formulation, makes routine characterizations with Ga^+ ions challenging since the material often segregates to the sample surface and masks signals from underlying species. Previous investigations using C_{60}^+ and SF_5^+ ion sources have shown it is possible to minimize the contribution of contamination layers like PDMS[25,31] as well as extract information that is more chemically relevant to the material in question.[26−32,37] Relatively few systems have been investigated using C_{60}^+, but its use shows promise in changing the way chemical information is extracted from the surface and bulk regions of polymers.[38] From these reported studies, it has been shown that C_{60}^+ ions increase the possibility that the SIBS polymer could be characterized in a three-dimensional format since the use of energetic, monatomic species like Ga^+ ions are known to lead to dehydrogenation and significant damage of backbone species using high primary ion doses.[39] Specifically, it is not possible to sputter ablate overlayers using this monatomic source, nor has it been possible to utilize it to depth profile polymeric materials. The relative enhancements of higher mass secondary ion peaks using C_{60}^+ primary ions are shown in Figure 3 (top). The significant enhancement in secondary ion intensity associated with the molecular ion of paclitaxel and higher mass fragments is clearly observed in the spectrum. Previous attempts to detect the molecular ion of paclitaxel using Ga^+ were unsuccessful even though the molecular ion was clearly observed in spectra from a pure reference compound.

Depth profiling results showing the intensity of secondary ion species associated with the polymer matrix plotted as a function of primary ion dose (C_{60}^+/cm^2) are shown in Figure 4. It is worth noting that all characteristic fragment ions from the polymer system show similar secondary ion intensity variations as a function of primary ion dose. As shown in Figure 4, the intensity profiles related to polystyrene and polyisobutylene possess slightly lower intensity in the near-surface region and then increase slightly before reaching a relatively uniform intensity (i.e., steady state) at higher ion doses. In contrast, the intensity profiles from PDMS- and paclitaxel-related species possess higher intensity in the near-surface region and then decrease before approaching a steady-state intensity after a primary ion dose of $\sim 2 \times 10^{13}$ ions/cm^2. These results suggest the surface region is somewhat enriched in PDMS and paclitaxel. If a matrix effect were to alter ion yields as a function of the sputtering process, then the relative intensities of fragment ions in the polymer could be affected. Another possibility includes the uniform enhancement/abatement

(37) Fletcher, J. S.; Conlan, X. A.; Jones, E. A.; Biddulph, G.; Lockyer, N. P.; Vickerman, J. C. *Anal. Chem.* **2006**, *78*, 1827−1831.
(38) Refer to cluster ion source manuscripts in: Proceedings of the SIMS XV International Conference 2005 in *Appl. Surf. Sci.* **2006**, *252* (19).
(39) Briggs, D. In *Practical Surface Analysis: Ion and Neutral Spectroscopy*, 2nd ed.; Briggs, D., Seah, M. P., Eds.; John Wiley & Sons: London, England, 1992; pp 367−423.

Table 1. Comparison of Select Secondary Ion Species from the Translute Polymer and Paclitaxel-Loaded Translute Polymer Matrixes Using Relatively Low and High C_{60}^+ Ion Doses[a]

			$I_{pk}/I_{97}(C_7H_{13})$			
			1.0×10^{14} ions/cm^2	1.0×10^{12} ions/cm^2	1.0×10^{14} ions/cm^2	1.0×10^{12} ions/cm^2
secondary ions	source	nominal mass	bulk no paclitaxel	surface no paclitaxel	bulk paclitaxel	surface paclitaxel
C_5H_3	PS	63	0.3	0.2	0.3	0.3
C_6H_3	PS	75	0.1	0.1	0.1	0.1
C_8H_7	PS	103	0.1	0.1	0.1	0.1
C_4H_8	PIB	56	0.4	0.4	0.4	0.5
C_6H_{11}	PIB	83	0.9	0.7	0.8	0.8
C_7H_{13}	PIB	97	1	1	1	1
C_8H_{15}	PIB	111	0.2	0.1	0.2	0.2
$C_{10}H_{17}$	PIB	137	4×10^{-2}	2×10^{-2}	4×10^{-2}	3×10^{-2}
$C_{14}H_{12}NO$	paclitaxel	210	xxx	xxx	3×10^{-3}	5×10^{-4}
$C_{15}H_{14}NO_2$	paclitaxel	240	xxx	xxx	4×10^{-3}	5×10^{-3}
$C_{16}H_{16}NO_4$	paclitaxel	286	xxx	xxx	1×10^{-3}	2×10^{-3}
$C_{29}H_{33}O_8$	paclitaxel	509	xxx	xxx	3×10^{-4}	6×10^{-4}
M + H	paclitaxel	855	xxx	xxx	6×10^{-5}	3×10^{-4}
$SiCH_3$	PDMS	43	1	8×10^{-1}	1	1
SiC_3H_9	PDMS	73	$2. \times 10^{-2}$	3×10^{-1}	2×10^{-2}	2×10^{-1}
$C_5H_{15}OSi_2$	PDMS	147	8×10^{-3}	1×10^{-1}	8×10^{-3}	6×10^{-2}
$C_5H_{15}O_3Si_3$	PDMS	207	4×10^{-3}	2×10^{-2}	4×10^{-3}	2×10^{-2}

[a] All peaks are the ratio of the sample to the isobutylene component species since it is a dominant component in the polymer. The slight variations in paclitaxel and PDMS intensities are attributed to its enhanced surface loading and subsequent removal during sputtering. Ratios are typically reproducible to ±10% using similar samples.

of secondary ions,[40] which may lead to similar intensity variations for each species. However, intensity profiles from fragment ions within the SIBS/paclitaxel system show intensity variations that are similar to those reported in Figure 4 and do not significantly vary from each other as a function of primary ion dose. Consequently, it is reasonable to assess that there is an enrichment of PDMS and paclitaxel at the surface of the SIBS polymer. At higher primary ion doses, the molecular ion signal associated with paclitaxel approaches the baseline intensity in the spectra. As a result, the molecular ion signal intensity observed above $\sim 1 \times 10^{13}$ ions/cm^2 is not considered adequate to establish the presence of the molecular ion at high primary ion doses. However, as observed in Figure 4, the intensity of the m/z 509 fragment peak from paclitaxel shows a similar distribution and is well above the baseline intensity. Although the molecular ion signal intensity is reduced at high primary ion doses, it is not coupled with a large increase in low-mass fragment ions as will be discussed below. At present, it is not possible to provide a more quantitative perspective, since sputter and ion yields as well as disappearance cross sections for the individual constituents are currently unknown. Further investigation into the solution-based release of paclitaxel, possible burst rates, and delivery lifetime may yield useful correlations to the above findings.

While contemplating sputter yields and disappearance cross sections, one may consider the relative changes C_{60}^+ primary ions induce during the bombardment process. Information pertaining to the three-dimensional distribution of species would be limited if the sample were significantly altered during the sputtering process. One indicator of surface modification induced by ion bombardment is an increase in low-mass fragments, a reduction in molecular ion species, or both.[39] To investigate this phenomenon further, we monitored the secondary ion intensities from a variety of species arising from the drug-loaded and non-drug-loaded polymer system. The secondary ion peak areas from select species, shown in Table 1, are representative of polystyrene, polyisobutylene, poly(dimethylsiloxane), and paclitaxel. These fragments were chosen to minimize the possibility of isobaric interferences between secondary ions from the respective components. By taking the ratio of the peak areas of these species to those from the base polymer, it is possible to obtain a better understanding of the relative intensity changes in the low- and high-mass regions of the spectrum under low and high primary ion dose conditions. In this instance, peak areas from representative fragment ions are divided by the C_7H_{13} intensity (i.e., peak area) from this polyisobutylene fragment. Although not reported in the table, utilization of other fragments from the same polymer as well as from polystyrene yielded the same trends. This process allows for direct comparison between samples with and without paclitaxel.[41] As a result, the values in Table 1 suggest the polymer backbone and components within the matrix are not significantly disrupted during the bombardment process, which is consistent with results reported by Weibel et al. for a series of homopolymers.[27] Notable changes in peak ratios associated with PDMS and paclitaxel are believed to arise from the sputter removal of these species from the surface. With respect to paclitaxel, another likely contributor is a decrease in high-mass species that may be associated with fragmentation pathways. Peak overlaps could also contribute to slight differences noted in the observed secondary ion intensity ratios.

To further investigate the possibility of matrix changes associated with ion beam bombardment, we expanded the comparisons by considering ion intensities summed from mass ranges in place of ratios using specific chemical moieties, which allowed us to incorporate nondescript peaks that are often overlooked or ignored

(40) Benninghoven, A. *Angew. Chem., Int. Ed. Engl.* **1994**, *33*, 1023−1043.

(41) Galuska, A. A. *Surf. Int. Anal.* **1994**, *21*, 703−710.

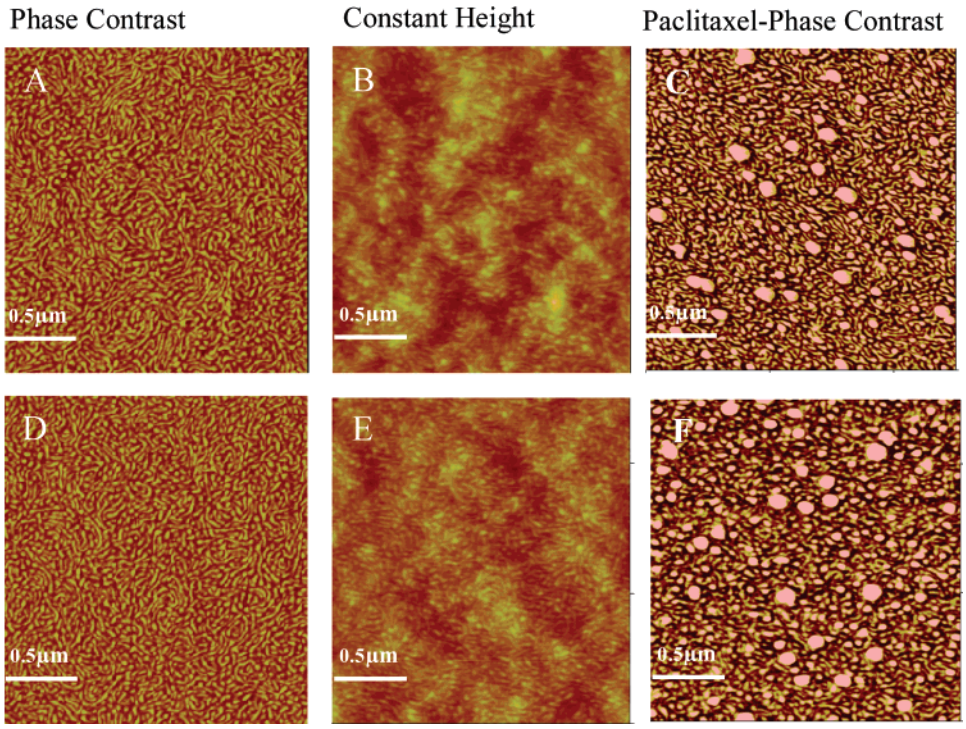

Figure 5. Atomic force microscopy images (all 2.5 μm × 2.5 μm) acquired from within the crater following a C_{60}^+ ion dose of 7 × 10^{14} C_{60}^+/cm^2 (A−C) and from control regions outside the sputter crater (D−F). Images A, B, D, and E show the Translute polymer without drug while images C and F show the paclitaxel containing Translute polymer. Images were obtained in phase contrast (A, C, D, F) and constant height (B, E) modes.

Table 2. Comparison of Secondary Ion Intensities from Larger Mass Regions To Assess Possible Accumulation of Ion Beam Damage Using Ga^+ and C_{60}^+ Primary Ions[a]

	relative intensities		
mass range (amu)	Ga (1 × 10^{12} ions/cm^2)[b]	C_{60} (1 × 10^{12} ions/cm^2)[b]	C_{60} (1 × 10^{14} ions/cm^2)[b]
0−100	8.9 × 10^{-1}	8.1 × 10^{-1}	8.4 × 10^{-1}
100−200	9.3 × 10^{-2}	1.4 × 10^{-1}	1.2 × 10^{-1}
200−300	1.6 × 10^{-2}	3.5 × 10^{-2}	2.1 × 10^{-2}
300−500	3.9 × 10^{-3}	1.3 × 10^{-2}	9.7 × 10^{-3}

[a] Summed intensities in the given range are divided by the total ion intensities for the respective spectra. Values suggest low accumulation of damage associated with C_{60}^+ sputtering. [b] Intensity of range/total ion intensity.

during data interpretation. The total ion intensity for the selected mass ranges divided by the total ion intensity for the given spectra are shown in Table 2. These results illustrate the differences between data generated by Ga^+ and C_{60}^+ utilizing primary ion doses of 1 × 10^{12} ions/cm^2 and further support the enhancement of higher mass secondary ion species using C_{60} primary ions. Moreover, comparison of these data to those obtained using primary ion doses of 1 × 10^{14} C_{60}^+ ions/cm^2 shows changes that are within a factor of 2 for the respective mass ranges. These findings are consistent with the removal of PDMS and paclitaxel at high primary ion doses and suggest fragmentation to low-mass species may be present but is limited.

In addition to possible increases of fragment ion intensities during sputtering, another indication that a surface is being altered or modified during the ion bombardment process is the creation of new surface topography.[42] To address this possibility, we employed atomic force microscopy to glean information about the individual components within the block copolymer as well as for the determination of surface roughness before and after sputtering. Phase contrast images obtained from 2.5 μm × 2.5 μm areas on the base polymer are shown in Figure 5. Data were obtained from multiple regions outside as well as within the sputter craters, and representative images are provided. Because of the distinct moduli and glass transition temperatures of polystyrene and polyisobutylene, the phase alterations of the oscillating AFM tip clearly define the copolymer domains.[43] In this system, the light areas correspond to polystyrene and the darker regions correspond to polyisobutylene. The domain structure of the copolymer is consistent with the nonsputtered surface even after primary ion doses of 7 × 10^{14} C_{60}^+ ions/cm^2. In addition to the relative phase information, constant height images of the pre- and postsputtered regions indicate that the surface topography changes slightly upon ion beam exposure. Specifically, root-mean-square roughness values for the copolymer show a relatively small increase (~10 nm) after the ion bombardment process. Increased surface roughness may result, at least in part, from differential sputtering associated with individual, copolymer blocks. However, additional work with the respective homopolymers would be required to conclusively correlate sputter yields with surface roughness. Consideration of the paclitaxel-containing polymer reveals similar root-mean-square roughness increases after C_{60}^+ sputtering as well a preserved domain structure. The right column

(42) Houlton, M. R.; Dosser, O. D.; Emeny, M. T.; Chew, A.; Sykes, D. E. In *Proceedings 8th International Conference on SIMS*; Benninghoven, A., Ed.; Wiley: London, England, 1992; pp 373−376.
(43) Puskas, J. E.; Antony, P.; Kwon, Y.; Kovar, M.; Norton, P. R. *Macromol. Symp.* **2003**, *183*, 191.

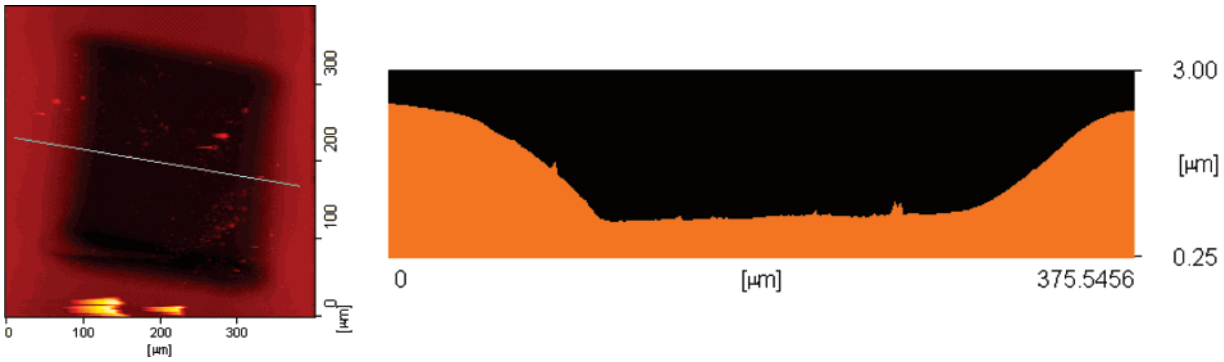

Figure 6. Profilometry scans showing relative crater size (left) and cross-sectional view along line shown in left image. The crater shown has a depth of ~1.5 μm.

images in Figure 5 clearly define the styrene/isobutylene domains discussed above, as well as the larger, circular regions associated the granular drug formulation. Based on these findings, the domain structure of the polymer appears well preserved after high, primary ion doses.[34]

An extension of these AFM studies was implemented through the use of a stylus profilometer. This technology allows us to record images and line scans from regions that encompassed entire sputter craters, which could not be performed in our imaging AFM system because of limited scan ranges associated with the instrumental design. Similar measurements are performed routinely in the semiconductor arena for measuring crater and device sizes on wafers. As shown in Figure 6, the cavity created in the SIBS copolymer using a 20-keV C_{60}^+ ion source has a relatively flat bottom. However, the crater edges are somewhat tapered, which is likely associated with lower current densities near the outer edges of the ion beam, which is ~30 μm in diameter. The relatively large, nonreproducible spikes observed in the images are believed to result from dust/debris deposited on the surface of the samples under ambient conditions since the work was conducted outside of a traditional clean room. Although the craters formed by C_{60}^+ ions appeared to be relatively flat and uniform, we attempted to minimize possible artifacts associated with the edge regions by directing the analysis beam within the central portion of the crater. Specifically, the width of the rastered area for the sputter probe is three to four times larger than the width of the rastered analysis probe.

After establishing the size and depth of the sputter craters, it is possible to calculate approximate sputter rates associated with the use of C_{60}^+. For the range of craters used in the above studies, the calculated sputter rates varied from 1.9 to 19 nm/s, resulting in relatively flat-bottom craters ~1−2 μm in depth. Corresponding ion currents range from 0.2 and 1.4 nA, respectively. The combination of high-mass sensitivity, low beam damage, reasonably high sputter rates, and flat-bottom craters (i.e., good depth resolution) has clearly established the use of C_{60}^+ ion sources for characterizing complex polymer systems. Future endeavors will undoubtedly extend toward investigations focused on explanted and biofouled materials since the mechanisms of attachment and growth vary significantly between systems and are poorly understood. Ultimately, the combination of molecular specificity, accomplished through high-mass resolution, coupled with the ability to probe the three-dimensional structure of materials will lead to a better understanding of biochemical properties within cellular organisms.

CONCLUSIONS

We believe the above results establish several advantages of using cluster (C_{60}^+) ion beams versus a conventional atomic ion source to characterize a drug-containing polymer sample. First, the lower energy per unit atom within the cluster ion and associated changes in energy transfer to the surface allow for higher detection sensitivities of surface species. This is marked by the significant enhancement of high-mass species within the reported C_{60}^+ data. However, more work is required to fully understand transformation probabilities, sputter yields, and disappearance/damage cross sections of related polymer species. In addition to enhanced secondary ion yields, the cluster ion beam showed a significant improvement in removing or minimizing the effects of overlayers. Specifically, it is possible to obtain molecular ion and fragment ion data from the paclitaxel/SIBS system at sufficient intensity with an abundance of poly(dimethylsiloxane) on the polymer surface. With respect to the three-dimensional distribution of species, we have determined that the surface of the polymer is slightly enriched with paclitaxel and PDMS based on the intensity curves and mass spectral analyses. After primary ion doses of ~2×10^{13} C_{60}^+ ions/cm^2, steady-state signals are observed and sustained through ion doses exceeding 6×10^{15} ions/cm^2. Interestingly, the use of C_{60}^+ to characterize this system does not appear to significantly alter the domain structure of the block copolymer as confirmed by AFM topography and phase contrast images. Previous attempts to characterize these materials as a function of depth using Ga^+ ion beams failed due to sample charging and surface damage associated with the high-energy, monatomic source. Based on these findings, the use of C_{60}^+ ion beams will greatly enhance the characterization of more complex polymers as well as ex vivo samples where the potential for surface contamination and biofouling is greatest.

ACKNOWLEDGMENT

We acknowledge Steve Kangas (Boston Scientific) for preparing the paclitaxel/SIBS films and John Newman (Evans Analytical Group) for use of the TRIFT III spectrometer. J.C. and N.W. also acknowledge the NIH and NSF for partial financial support of this work.

Received for review August 14, 2006. Accepted October 3, 2006.

AC0615089